Model improvements to 'Quantitative phase-field approach for simulating grain growth in anisotropic systems with arbitrary inclination and misorientation dependence'

Nele Moelans*
KU Leuven, Department of Materials Engineering,
Kasteelpark Arenberg 44,
bus 24.50, 3001 Leuven, Belgium.

(Dated: March 12, 2021)

In the papers [PRL 101, 025502(2008); PRB 78, 024113 (2008)], the author proposed a quantitative phase-field model for polycrystalline structures with misorientation and inclinatin dependence of the grain boundary properties. A detailed analysis on the relation between model parameters and the boundary properties obtained in the simulations was presented, resulting in a procedure to compute an appropriate set of model parameters for given misorientation and inclination dependence of the grain boundary energy and mobility. An important feature of the model is that third phases or ghost phases at boundaries are completely suppressed without the need of adding complex higher order terms in the energy function. In later studies, it was found that the wetting at triple junctions and the behavior of triple junctionss with an angle deviating largely from 120° were not reproduced correctly. The aim of this paper is to give an improved model resolving these issues. An alternative, and even simpler, procedure to determine the misorientation dependent input parameters and describe inclination dependence for the same model is given. The new approach is derived in a fully variational way and still ghost phases at grain boundaries are suppressed. The model contains a parameter to control the length sclale of the diffuse interface without affecting the grain boundary properties; however, we had to relaxe the constraint of equal diffuse interface width along all boundaries. It is verified for the new approach that accurate triple junction angles are obtained under all conditions, also for large differences between the grain boundary energies resulting in triple junction angles that deviate largely from 120 and the variations in grain boundary width associated with variations in grain boundary energy are quantified. It is shown that grain boundary wetting is reproduced. Moreover, 3 alternative ways to include inclination dependence are compared.

I. INTRODUCTION

In the papers [**?**] and [], the author presented a model for grain growth simulations in systems with inhomogeneous grain boundary properties and derived quantitative relations between the model parameters and the physcial grain boundary energy and mobility of the boundaries. The boundary energy was assumed to be dependent on the difference in orientation between the adjacent grains (misorientation dependence) and on the inclination of the grain boundary. A procedure was proposed to determine a set of input parameter for a given set of grain boundary properties. The model and parameter determination procedure were derived in such a way that the diffuse interface width can be chosen independent from the boundary properties and is constant along all boundaries, even for varying grain boundary properties. Morover, irrespective of the ratio between the grain boundary energies, spurious phases at grain boundaries, which used to be an important problem in other phase-field models [], are naturally suppressed with this model without the need to add complex third order interaction terms. The model was validated for a wide range of grain boundary energies and triple junction angles and accurate result could be obtained. Moreover, with the introduction of an appropriate tilting function, the model was extended to multi-component and multi-phase systems [], leading to wide application of the model formulation.

However, in later studies, it was observed that triple junction angles deviating largely from 120°, could not be reproduced accurately and even resulted in unphysical behavior for the proposed model parameter relations. Moreover, the proposed approach to include inclination dependence in the grain boundary energy is highly complex for cases with intermediate to strong anisotropy. Here, we present a solution for these artefacts. We show that the unphysical triple junction behavior can be removed and the accuracy with which triple junction angles are reproduced can be drastically improved, without any change in the form of the model equations, simply by a different interpretation of the model parametes []. The new formulation increases the applicability of the earlier model towards systems with strong anisotropy. Three alternatives to include inclination dependence are discussed and compared.

In the remainder of the paper, first, a summary of the original model formulation and parameter relations is given. Then, the necessary model modifications are discussed and a new procedure to relate the model parameters to the pysical grain boundary properties is presented, first only considering misorientation dependence of the grain boundary properties. The merits are illustrated by means of numerical simulations. Next, 3 different ways are discussed and compared to include inclination depen-

* nele.moelans@kuleuven.be

dence in the improved model.

II. THE ORIGINAL MODEL

In the considered phase-field model for grain growth, orientation space is discretized and the different discrete grain orientations are represented using a large set of non-conserved field variables, or phase-fields

$$\eta_1(\mathbf{r},t), \eta_2(\mathbf{r},t), \eta_3(\mathbf{r},t), \ldots, \eta_i(\mathbf{r},t), \ldots \eta_p(\mathbf{r},t).$$

Within each grain, one of the phase-fields, the one representing the particular grain orientation, equals one, while the other phase-fields are equal to zero. Grain orientation is assumed to be constant within a grain, although it is possible to consider subboundaries with low misorientation []. At the grain boundaries, the 2 phase-field variables representing the adjacent grains vary smoothly between the values zero and one within a relatively thin diffuse interface region. For numerical reasons, we have defined the width of this diffuse region, $\ell_{i,j}$, based on the steepest gradient to the phase-field variables within this region, namely as

$$\ell_{i,j} = \frac{1}{|(\mathrm{d}\eta_i/\mathrm{dx})_{\mathrm{x}=0}|} = \frac{1}{|(\mathrm{d}\eta_j/\mathrm{dx})_{\mathrm{x}=0}|}.$$

This concept is illustrated in Fig xx.

The evolution equations of the phase-field variables are derived starting from the time-dependent Ginzburg-Landau equation

$$\frac{\partial \eta_i(\mathbf{r},t)}{\partial t} = -L(\eta_1, \eta_2, \ldots, \eta_p)\frac{\delta F(\eta_1, \eta_2, \ldots, \eta_p)}{\delta \eta_i(\mathbf{r},t)} \quad (1)$$

for all $i = 1 \ldots p$ phase-field variables. The kinetic coefficient L is formulated as a function of the order parameters as

$$L(\eta_1, \eta_2, \ldots, \eta_p) = \frac{\sum_{i=1}^{p}\sum_{j>i}^{p} L_{i,j}(\phi_{i,j})\eta_i^2\eta_j^2}{\sum_{i=1}^{p}\sum_{j>i}^{p}\eta_i^2\eta_j^2}. \quad (2)$$

where the parameters $L_{i,j}$ are related to the mobility of the grain boundary between a grain with orientation i and one with orientation j. Misorientation dependence can thus be introduced taking different values for the $L_{i,j}$. The $L_{i,j}$ can be a function of $\phi_{i,j}$, the normalized vector that specifies the orientation of the normal to the grain boundary between grains with orientations i and j, to include inclindation dependence of grain boundary mobility. The direction of the grain boundary normal $\phi_{i,j}$ can be computed from the local gradients of the phase-field variables $\nabla\eta_i$ and $\nabla\eta_j$:

$$\phi_{i,j} = \frac{\nabla\eta_i - \nabla\eta_j}{|\nabla\eta_i - \nabla\eta_j|}.. \quad (3)$$

Since at each boundary only two phase-field variables are different from zero, only the term $L_{i,j}\eta_i^2\eta_j^2$ remains in the numerator and $\eta_i^2\eta_j^2$ in the nominator when at a boundary between grains i and j, resulting in $L = L_{i,j}(\phi)$ at this boundary.

The free energy functional F has the form

$$F = \int_V \Big[m f_0(\eta_1, \eta_2, \ldots, \eta_p) + \frac{\kappa(\eta_1, \eta_2, \ldots, \eta_p)}{2}\sum_{i=1}^{p}(\nabla\eta_i)^2 \Big] \mathrm{d}V, \quad (4)$$

with

$$f_0(\eta_1, \eta_2, \ldots, \eta_p) = \sum_{i=1}^{p}\left(\frac{\eta_i^4}{4} - \frac{\eta_i^2}{2}\right) + \sum_{i=1}^{p}\sum_{j>i}^{p}\gamma_{i,j}(\phi)\eta_i^2\eta_j^2 + \frac{1}{4}, \quad (5)$$

and the energy gradient coefficient

$$\kappa(\eta_1, \eta_2, \ldots, \eta_p) = \frac{\sum_{i=1}^{p}\sum_{j>i}^{p}\kappa_{i,j}(\phi_{i,j})\eta_i^2\eta_j^2}{\sum_{i=1}^{p}\sum_{j>i}^{p}\eta_i^2\eta_j^2}. \quad (6)$$

formulated as a function of the phase-field variables and energy gradient coefficients $\kappa_{i,j}$ related to properties of the boundary between grains i and j using a similar expression as for the kinetic coefficient L,

Irrespective of the model parameter values, f_0 has multiple degenerate minima located at

$$(\eta_1, \eta_2, \ldots, \eta_p) = (\pm 1, 0, \ldots, 0), (0, \pm 1, 0, \ldots, 0), \ldots, (0, \ldots, 0, \pm 1)$$

where $f_0 = f_{0,\min} = 0$, corresponding to the different grain orientations. It equals zero within grains and has a positive value at the diffuse grain boundaries contributing to the grain boundary energy.

The coefficients $\gamma_{i,j}$ (Eq.30) and $\kappa_{i,j}$ (Eq.6) are related to the energy and thickness of a boundary between a grain with orientation i and one with orientation j. Note again, that, at a boundary between grains i and j, only the terms in $\eta_i^2\eta_j^2$ in all double summations in Eqs. (30) and (Eq.6) differ from zero. The misorientation dependence of the grain boundary energy can thus be considered by the different $\kappa_{i,j}$ and $\gamma_{i,j}$. The $\gamma_{i,j}$ and $\kappa_{i,j}$ themselves can be a function of the local inclination of the grain boundary $\phi_{i,j}$ when grain boundary energy is inclincation dependent. The coefficient m is a constant and affects the grain boundary energy and diffuse interface width of all boundaries.

Combinin Eq. (1) and Eq. (29), following evolution equation for the phase field variables $\eta_i(\mathbf{r},t)$ can be ob-

tained in the absence of inclination dependence

$$\frac{\partial \eta_i(\mathbf{r},t)}{\partial t} = -L(\eta_1,\eta_2,\ldots,\eta_p)\Bigg[m\left(\eta_i^3 - \eta_i + 2\eta_i \sum_{j\neq i}^{p} \gamma_{i,j}\eta_j^2\right) -\kappa(\eta_1,\eta_2,\ldots,\eta_p)\nabla^2\eta_i\Bigg], \quad (7)$$

for $i = 1 \ldots p$. To obtain this evolution equation, the η-dependence of $\kappa(\eta_1,\eta_2,\ldots,\eta_p)$ was omitted when taking the derivative of $\frac{\delta F(\eta_1,\eta_2,\ldots,\eta_p)}{\delta \eta_i(\mathbf{r},t)}$. This non-variational treatment of the η-dependence of $\kappa(\eta_1,\eta_2,\ldots,\eta_p)$ was needed to avoid the presence of spurious phases at higher energy boundaries, as elaborated in []. In the presence of inclination dependence, the dependence of the coefficients κ and γ on the gradients of the phase-fields $\nabla\eta_i(\mathbf{r},t)$ must be considered as well, resulting in lengthier equation given in []).

Misorientation dependence in grain boundary energy and mobility is thus introduced in a discrete way through the model parameters $\kappa_{i,j}$, $\gamma_{i,j}$ and $L_{i,j}$, while for each misorientation, the parameters can be a continuous functions of the grain boundary inclination $\phi_{i,j}$.

For each grain boundary, the following relations between its physical grain boundary energy $\sigma_{i,j}$, mobility $\mu_{i,j}$ and thickness $\ell_{i,j}$, on the one hand, and the model parameters m, $\kappa_{i,j}$, $\gamma_{i,j}$ and $L_{i,j}$, on the ohter hand, were obtained after carefull analytical and numerical analysis,

$$\sigma_{i,j} = g(\gamma_{i,j})\sqrt{\kappa_{i,j} m} \quad (8a)$$

$$\ell_{i,j} = \sqrt{\frac{\kappa_{i,j}}{m f_{0,interf}(\gamma_{i,j})}} \quad (8b)$$

$$\mu_{i,j} = \frac{L_{i,j}\kappa_{i,j}}{\sigma_{i,j}} = \frac{L_{i,j}}{g(\gamma_{i,j})}\sqrt{\frac{\kappa_{i,j}}{m}}, \quad (8c)$$

with $\ell_{i,j}$ determined according to Eq. (1). or, alternatively,

$$\kappa_{i,j} = \sigma_{i,j}\ell_{i,j}\frac{\sqrt{f_{0,\mathrm{interf}}(\gamma_i,j)}}{g(\gamma_i,j)} \quad (9a)$$

$$L_{i,j} = \frac{\mu_{i,j}}{\ell_{i,j}}\frac{g(\gamma_{i,j})}{\sqrt{f_{0,\mathrm{interf}}(\gamma_{i,j})}} \quad (9b)$$

$$m = \frac{\sigma_{i,j}}{\ell_{i,j}}\frac{1}{g(\gamma_{i,j})\sqrt{f_{0,\mathrm{interf}}(\gamma_{i,j})}},$$

with i and j refering to the order parameters representing the two adjacent grains. The values of the functions $g(\gamma_{i,j})$ and $f_{0,\mathrm{intaerf}}(\gamma_{i,j})$ were evaluated numerically as a function of the value of $\gamma_{i,j}$. A list of the data is available online []. For $0.5 > \gamma_{i,j} > 40$, following fourth order polynomial firs well the data points obtained for $1/\gamma$ as a function of the square root of g, i.e. g^2,

$$\frac{1}{\gamma} = -3.0944[g^2]^4 - 1.8169[g^2]^3 + 10.323 * [g^2]^2 - 8.1819[g^2] + 2.0033, \quad (10)$$

and following sixth order polynomial fits well the data points for f_{interf} as a function of $1/\gamma$,

$$f_{interf} = pp1 * (\frac{1}{\gamma})^6 + pp2 * (\frac{1}{\gamma})^5 + pp3 * (\frac{1}{\gamma})^4 \quad (11)$$

$$+pp4 * (\frac{1}{\gamma})^3 + pp5 * (\frac{1}{\gamma})^2 + pp6 * (\frac{1}{\gamma})^1 + pp7. \quad (12)$$

Nog fitten These polynomial relations can be used in an algorithm to compute the model parameters for given grain boundary properties. A graph is shown in figure 1.

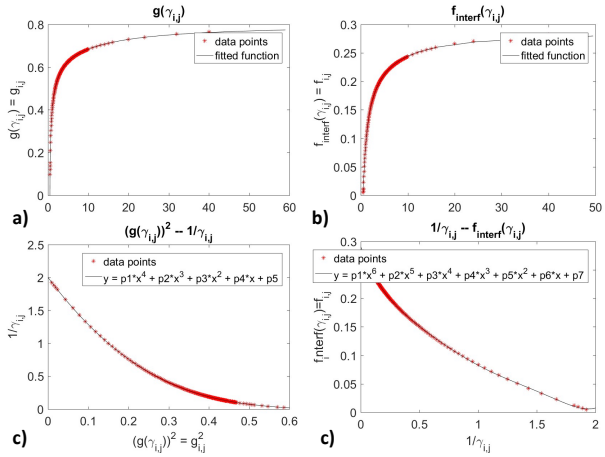

FIG. 1. a) Plot of the values of $g(\gamma)$
b) same data points but plotted as $1/\gamma$ as a function of g^2. A fifth order polynomial with coefficients as given in Eq xx fits the data points well. c) d)

With p grain orientations, there can be $0.5 * p * (p-1)$ different types of boundaries present in the simulation. The phase-field model then contains $3 \times 0.5 * p * (p-1) + 1$ model parameters ($\gamma_{i,j}$, $\kappa_{i,j}$, $L_{i,j}$ and m) to fix $3 \times 0.5 * p * (p-1)$ grain boundary properties ($\sigma_{i,j}$, $\ell_{i,j}$ and $\mu_{i,j}$). The model therefore contains sufficient model parameter to specify the diffuse interface width $\ell_{i,j}$ for numerical convenincen for each boundary independent without affecting the grain boundary properties and independent of the width of other boundaries. Therefore, in order to resolve the movement of all boundaries with a same accuracy, it was proposed to take a homogeneous grain boundary width along all boundaries, i.e. $\ell_{i,j}(\phi_{i,ju}) = \ell_{gb}$, even when the grain boundary properties vary. An algorithm was proposed to compute the model parameters for a

given set of $\sigma_{i,j}$ and $\mu_{i,j}$ and one common diffuse interface width ℓ_{gb}. For this considered model parameter choice, there is still one degree of freedom. Various sets of model parameter values can represent a same set of physical grain boundary properties (and will thus lead to the same simulation results). It is best to chose a set of paremeter values with the $\gamma_{i,j}$ as much as possible around the value 1.5, for which symmetrical phase-field profiles are obtained at the interface (*add picture to illustrate this + also to illustrate grain representation for the introduction + illustrate definition of diffuse interface width*).

With the proposed model formulation and procedure to determine the model parameter, it is possible to obtain highly accurate grain boundary kinetics and accurate triple junction angles for angles between xxx and xxx degree, as shown in []. The fact that the derivation of the evolution equations is not variational with respect to the η-dependence of $\kappa(\eta_1, \eta_2, \ldots, \eta_p)$ did not affect the results for the considered conditions. In later studies using the model, unphysical effects were however observed for very large and very small triple junction angles, i.e. when the ratio between the grain boundary energies of the boundaries joining at the triple junction is close to or exceeds 2. Firstly, wetting could not be reproduced with the model. Secondly, for very high triple junction angles (towards 180°), the triple junction was found to move in the opposite direction than physically expected. *add or refer to illustrating picture.* It is very likely that these unphysical effects are devoted to the non-variational treatment of the η-dependence of κ in the evolution equations.

FIG. 2. Unphysical effects at triple junctions observed for the original model formulation for large differences in grain boundary energies. For geometry 5, $\sigma_{1,2}$ = and $\sigma_{1,2}$ = and according to Young's law a triple junction angle $2 * \theta = xxx$ is expected. However, this angle cannot be reproduced and, even worse, the triple junction moving upwards instead of downwards. For geometry 6, $\sigma_{1,2}$ = and $\sigma_{1,2}$. It is thus expected that grain 3 wets the boundary between grains 1 and 2. The model cannot reproduced this. The angle remains at xxx degrees. See table xxx for more details about the simulation configuraitons 5 and 6.

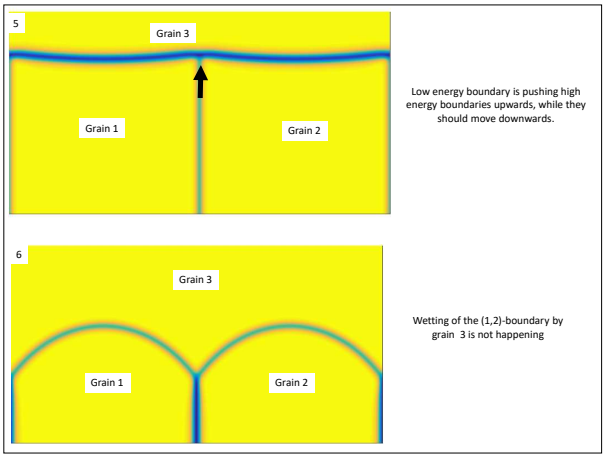

III. NEW APPROACH TO INLCUDE MISORIENTATION DEPENDENCE OF GRAIN BOUNDARY PROPERTIES

The prerequisites of the new model formualtion are the following.

1) A fully variational derivation of the evolution equations is crucial to reproduce triple junction angle behavior correctly irrespective of the ratios of the grain boundary energies of the joining grain boundaries.

2) Spurious phases at grain boundaries must be avoided irrespective of the ratios of the grain boundary energies, since their presence affects the grain boundary properties and may drag grain boundary migration.

3) To allow for large scale simulations, it must be possible to adapt the length scale of the diffuse grain boundary width independent from the grain boundary energies and mobilities.

After profound mathematical analysis of the equations, we concluded that it is most probably impossible to find an expression for the gradient energy contribution $\kappa(\eta_1, \eta_2, \ldots, \eta_p) \sum_i^p (\nabla \eta_i)^2$ in the free energy that allows for both a fully variational derivation and complete suppression of spurious phases for any combination of grain boundaries energies. Therefore, it is decided that the most straightforward solution is to take κ constant in the free energy function (Eq. 29), i.e. take $\kappa_{i,j} = \kappa, \forall i, j$. For $\kappa(\eta_1, \eta_2, \ldots, \eta_p) = cte$, the following evolution equations can be obtained from xx and xx, using a fully variational derivation, for $i = 1 \ldots p$

$$\frac{\partial \eta_i(\mathbf{r}, t)}{\partial t} = -L(\eta_1, \eta_2, \ldots, \eta_p) \Bigg[m \left(\eta_i^3 - \eta_i + 2\eta_i \sum_{j \neq i}^{p} \gamma_{i,j} \eta_j^2 \right) - \kappa \nabla^2 \eta_i \Bigg]. \tag{13}$$

The misorientation dependence of the grain boundary energy can still be introduced through the model parameters $\gamma_{i,j}$. The parameter relations (Eqs. (8)) and polynomial fits (10) and (12), derived for the original model, are still valid, when taking $\kappa_{i,j} = \kappa$ equal for all boundaries, giving

$$\sigma_{i,j} = g(\gamma_{i,j}) \sqrt{\kappa m} \tag{14a}$$

$$\ell_{i,j} = \sqrt{\frac{\kappa}{m f_{0,interf}(\gamma_{i,j})}} \tag{14b}$$

$$\mu_{i,j} = \frac{L_{i,j} \kappa}{\sigma_{i,j}} = \frac{L_{i,j}}{g(\gamma_{i,j})} \sqrt{\frac{\kappa}{m}}, \tag{14c}$$

TABLE I. List of combinations of grain boundary energies considered in the triple junction simulations and associated model parameters values as determined with the original procedure as described above. The grain boundary mobility $\mu_{i,j} = 1$ was taken for all boundaries. Note that the diffuse width of all boundaries is equal to 1.6.

n°	$\sigma_{1,2}$	$\sigma_{1,3} = \sigma_{2,3}$	$\kappa_{1,2}$	$\kappa_{1,3} = \kappa_{2,3}$	m	$\gamma_{1,2}$	$\gamma_{1,3} = \gamma_{2,3}$	$L_{1,2}$	$L_{1,3} = L_{2,3}$	ℓ_{gb}
iso	0.25	0.25	0.3	0.3	0.9375	1.5	1.5	0.833	0.833	1.6
1	0.2	0.25	0.2396	0.3	0.9375	1.1629	1.5	0.8348	0.8334	1.6
2	0.25	0.2	0.3	0.2396	0.9375	1.5	1.1629	0.8334	0.8348	1.6
3	0.15	0.25	0.1787	0.3	0.9375	0.9211	1.5	0.8395	0.8334	1.6
4	0.25	0.15	0.3	0.1787	0.9375	1.5	0.9211	0.8334	0.8395	1.6
5	0.15	0.4	0.1777	0.4730	0.9375	0.9250	3.8869	0.8440	0.8457	1.6
6	0.4	0.15	0.4730	0.1777	0.9375	3.8869	0.9250	0.8457	0.8440	1.6
7	0.15	0.75	0.1788	0.8844	1.6875	0.6898	4.4197	0.8389	0.8480	1.6

TABLE II. Triple junction angles obtained with both the original and new model formulation and parameter choice. Both values are compared with the angle expected from theory. The angles were measured from simulations of a 2 grain structure as shown in Fig (T-geometry).

n°	$2 * \theta_{orig}$	$2 * \theta_{new}$	$2 * \theta_{theory}$
iso	118.36°	118.36°	120°
1	131.85°	131.66°	132.84°
2	106.82°	100.21°	102.64°
3	149.82°	143.94°	145.08°
4	91.09°	61.2°	67.11°
5	unphysical	157.35°	158.39°
6	68.95°	wetting	wetting
7	unphysical	166.98°	168.52°

When considering p grain orientations, the new approach contains $2 \times 0.5 \times p \times (p-1) + 2$ model parameters ($\gamma_{i,j}$, $L_{i,j}$, κ, and m) to fix $3 \times 0.5 \times p \times (p-1)$ grain boundary properties ($\sigma_{i,j}$, $\ell_{i,j}$ and $\mu_{i,j}$). There are thus insufficient model parameters to specify the width of each grain boundary individually. In order to guarantee prerequisites 1 and 2, we had to give up the feature of constant diffuse interface width along all boundaries of the original model. Still, after fixing the grain boundary energy and mobility of all different types of boundaries (requiring $2 \times 0.5 \times p \times (p-1)$ model parameters), 2 model parameters remain which can be used to adjust the overall length scale of the diffuse interface. Although there will be variations in width along the boundaries, the diffuse interface width of all boundaries can be scaled with a same factor by varying the ratio $\sqrt{\kappa/m}$. This alternative parameter choice was already applied, but without giving much details, in recent studies [].

A procedure to compute all model parameters for a set of grain boundary energies $\sigma_{i,j}$ and mobilities $\mu_{i,j}$ and a minimum interface width required for the numerical accuracy ℓ_{min}, could be as follows

1. First consider the boundary with the highest interface energy $\sigma_{i,j} = \sigma_{max}$. Compute the model parameters for this boundary using parameter relations (14) and taking $\gamma = 1.5$ (or the maximum γ-value γ_{max} to be used in the simulations) and $\ell_{i,j} = \ell_{min}$

   $\rightarrow$ κ and m to be used for all boundaries and $\gamma_{i,j}$ and $L_{i,j}$ for the boundary with maximum energy are obtained.

2. Then, for all boundaries with energy $\sigma_{i,j}$ and mobility $\mu_{i,j}$ $(i = 1 \ldots p, j = i+1 \ldots p)$

   (a) Compute the model parameters $\gamma_{i,j}$ and $L_{i,j}$ using parameter relations (14) with $\sigma_{i,j}$ and $\mu_{i,j}$ of the boundary and κ and m as computed in step 1.

   (b) Optionally compute the diffuse widht $\ell_{i,j}$ using Eq. (14b)

An implementation of this adapted procedure to calculate the model parameters for a given set of grain boundary energies and mobilities is given in the supplementary material.

Table III gives possible sets of model parameter values considering 7 different combinations of grain boundary energies for triple junction angle simulations. Boundaries with a different energy have a different width, and the boundary with the highest energy always has the smallest width; however, the maximum variation is xxx. Note, also that although the grain boundary mobility of all boundaries is taken the same, the values of $L_{i,j}$ for boundaries with a different energy are different. This follows from Eq. (14c).

For the new approach, the simulated triple junction angles are depicted in Figure 3. The triple junction angles are close to the theoretical values (see additional material for an explanation on how triple junction angles were measured). For configuration 6, grain 3 wets the boundary between grains 1 and 2 as expected since $\sigma_{1,2} > 2\sigma_{1,3} = 2\sigma_{2,3}$. Also for configurations 5 and 7 with a triple junction angle around and above 160°, the angle is reproduced accurately and the junction is moving in the right direction. Table xx compares the triple junction angles as obtained with the original and the new approach with the theoretical values. While both models have a similar accuracy for triple junction angles around 120°, the new model outperforms the original for very small and very large angles.

TABLE III. List of combinations of grain boundary energies considered in the triple junction simulations and associated model parameters values as determined with the new procedure to include misorientation dependence. The grain boundary mobility $\mu_{i,j} = 1$ was taken for all boundaries. *compute and complete diffuse interface width for all boundaries*

n	$\sigma_{1,2}$	$\sigma_{1,3} = \sigma_{2,3}$	κ	m	$\gamma_{1,2}$	$\gamma_{1,3} = \gamma_{2,3}$	$L_{1,2}$	$L_{1,3} = L_{2,3}$	$\ell_{1,2}$	$\ell_{1,3} = \ell_{2,3}$
iso	0.25	0.25	0.3	0.9375	1.5	1.5	0.833	0.833	1.6	1.6
1	0.2	0.25	0.3	0.9375	0.9594	1.5	0.6667	0.8333	1.6	
2	0.25	0.2	0.3	0.9375	1.5	0.9594	0.8333	0.6667	1.6	
3	0.15	0.25	0.3	0.9375	0.7063	1.5	0.5	0.8333		1.6
4	0.25	0.15	0.3	0.9375	1.5	0.7063	0.8333	0.5	1.6	
5	0.15	0.4	0.36	1.125	0.6328	5.1364	0.4167	1.1111		
6	0.4	0.15	0.36	1.125	5.1364	0.6328	1.1111	0.4167		
7	0.15	0.75	0.6	1.8750	0.5424	13.7765	0.25	1.25		

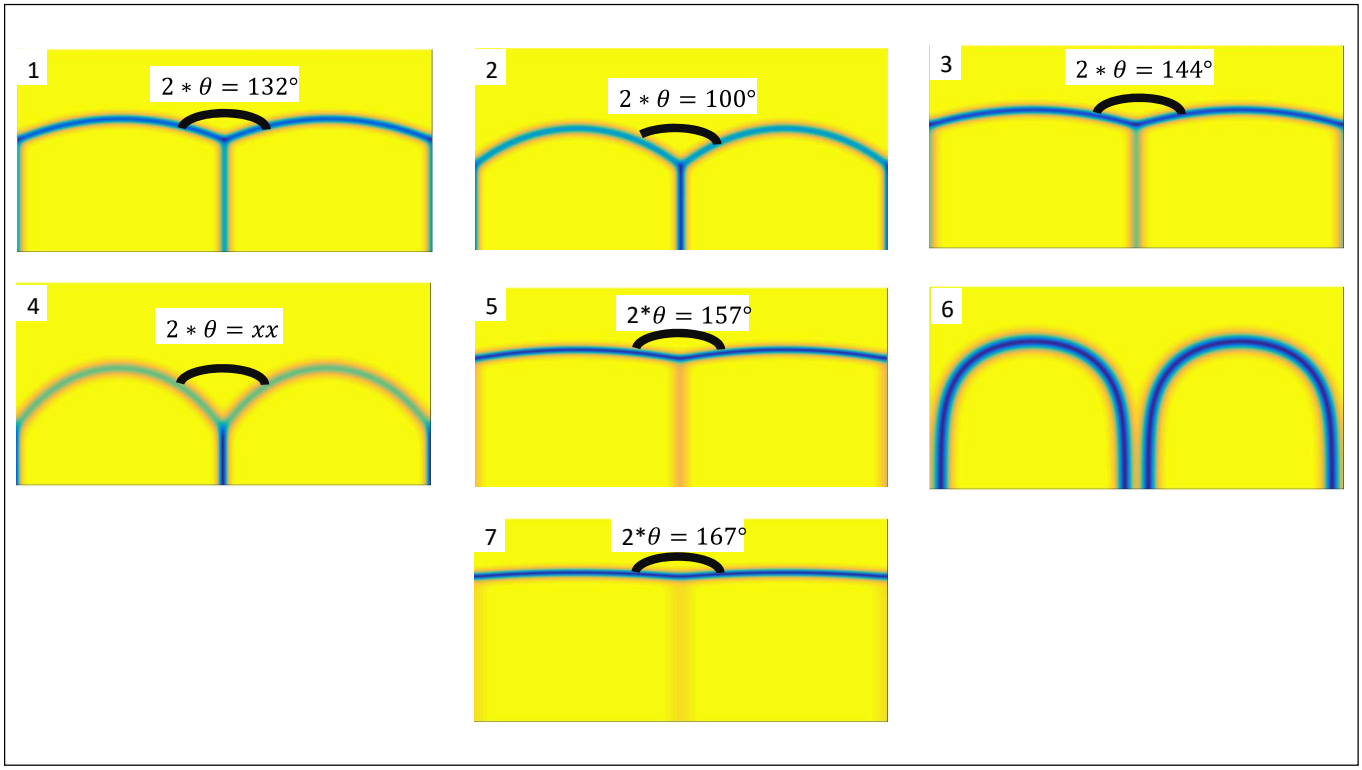

FIG. 3. Triple junction angles as obtained with the new model formulation for the 7 sets of grain boundary energies listed in table III. The system size is 200 × 400, grid spacing $\Delta x = 0.2$. Periodic boundary conditions are assumed along the vertical boundaries and Neumann along the horizontal. The junction is moving downwards under the curvature driving force of the boundaries.

IV. THREE APPROACHES TO INCLUDE INCLINATION DEPENDENCE IN THE NEW APPROACH

We assume that the inclination dependence of the grain boundary energies and mobilities of the different boundaries is known and can be written in the form

$$\sigma_{i,j}(\phi_{i,j}) = \sigma^0_{i,j} f^\sigma_{i,j}(\phi_{i,j}) \tag{15}$$

$$\mu_{i,j}(\phi_{i,j}) = \mu^0_{i,j} f^\mu_{i,j}(\phi_{i,j}) \tag{16}$$

with ϕ the inclination, i.e. the unit normal to the grain boundary, which can be obtained from the gradients of the phase-field variables $\nabla\eta_i$ and $\nabla\eta_j$ using Eq. (3). In

this paper, we will consider two frequently used function to describe 2-dimensional inclination dependence, namely

$$f^{\sigma}_{i,j} = 1 + \delta_{i,j} \cos\left(n_{i,j}\left(\phi'_{i,j} - \phi_0\right)\right)$$

with $\delta_{i,j}$ the strength of the inclination dependence, $n_{i,j}$ refers to n- fold symmetry, $\phi'_{i,j}$ the angle between the x-axis and the unit normal to the grain boundary $\phi_{i,j}$ and ϕ_0 an offset angle determining the orientation with highest energy, which can be computed from the gradients of the phase-field variables $\nabla\eta_i$ and $\nabla\eta_j$ as

$$\phi'_{i,j} = \arctan(\frac{\nabla_y\eta_i - \nabla_y\eta_j}{\nabla_x\eta_i - \nabla_x\eta_j}). \tag{17}$$

A. Through energy gradient contribution

In a first alternative, inclination dependence is introduced in the gradient energy term in the free energy functional and in the kinetic coefficients $L_{i,j}$ as follows

$$F = \int_V \left[m f_0(\eta_1, \eta_2, \ldots, \eta_p) + \frac{\kappa(\phi)}{2} \sum_{i=1}^{p} (\nabla\eta_i)^2 \right] \mathrm{d}V, \tag{18}$$

with

$$\kappa(\phi) = \kappa^0 \frac{\sum_{i=1}^{p}\sum_{j>i}^{p}\left[f^{\sigma}_{i,j}(\phi_{i,j})\right]^2 \eta_i^2\eta_j^2}{\sum_{i=1}^{p}\sum_{j>i}^{p}\eta_i^2\eta_j^2} \tag{19}$$

and

$$L(\eta_1, \eta_2, \ldots, \eta_p) = \frac{\sum_{i=1}^{p}\sum_{j>i}^{p} L_{i,j}(\phi_{i,j})\eta_i^2\eta_j^2}{\sum_{i=1}^{p}\sum_{j>i}^{p}\eta_i^2\eta_j^2}. \tag{20}$$

with

$$L_{i,j}(\phi_{i,j}) = L^0_{i,j}\frac{f^{\mu}_{i,j}(\phi)}{f^{\sigma}_{i,j}(\phi)} \tag{21}$$

The evolution equations for the phase-field variables η_i are obtained in a fully variation way starting from Eq. (1) and using Eqs. (18) and (20), giving

$$\frac{\partial\eta_i(\mathbf{r},t)}{\partial t} = -L(\eta_1, \eta_2, \ldots, \eta_p)\Bigg[m\left(\eta_i^3 - \eta_i + 2\eta_i\sum_{j\neq i}^{p}\gamma_{i,j}\eta_j^2\right) + \frac{1}{2}\frac{\partial\kappa}{\partial\eta_i}\sum_{i=1}^{p}(\nabla\eta_i)^2 - \nabla\cdot\left(\kappa\nabla\eta_i + \frac{1}{2}\frac{\partial\kappa}{\partial\nabla\eta_i}\sum_{i=1}^{p}(\nabla\eta_i)^2\right)\Bigg]. \tag{22}$$

Note that, different from the original model, the prefactor κ^0 in the energy gradient coefficient is taken as a constant, the same value for all boundaries, in this new approach, while the inclination dependent factor can be different for different boundaries and is interpolated using the cross summations. Thanks to the constant value of the prefactor κ^0, the presence of spurious phases at grain boundaries is suppressed, also with a fully variational derivation of the evolution equations.

From the thin interface analysis in [PRB2008], it follows that the inclination is constant throughout the diffuse interface along the grain boundary normal, and therefore the parameter relations (8) remain valid. From these relations, it follows, that the square of the inclination dependent part of the grain boundary energy $[f^{\sigma}_{i,j}(\phi_{i,j})]^2$ has to be used in the gradient energy part to recover the expected inclination dependence $f^{\sigma}_{i,j}(\phi_{i,j})$ for $\sigma_{i,j}$, since $\sigma_{i,j}$ is proportional to $\sqrt{\kappa[f^{\sigma}_{i,j}(\phi_{i,j})]^2}$ (see Eq. (8a)). The inclination depence of the grain boundary mobility $f^{\mu}_{i,j}(\phi_{i,j})$ can be simply introduced through the kinetic coefficients $L_{i,j}$, since $\mu_{i,j}$ is proportional to $L_{i,j}$ (see Eq. (8c). However, becuase of the square of the inclination dependent function in the energy gradient contribution, it is needed to divide $L_{i,j}$ by the inclination dependent part $f^{\sigma}_{i,j}(\phi_{i,j})$ of the grain boundary energy to recover the correct inclination dependence of $\mu_{i,j}$. For the proposed model, the following parameter relations are thus obtained

$$\sigma_{i,j}(\phi_{i,j}) = \sigma^0_{i,j} f^{\sigma}_{i,j}(\phi_{i,j}) = g(\gamma_{i,j})\sqrt{\kappa^0 m} f^{\sigma}_{i,j}(\phi_{i,j}) \tag{23a}$$

$$\ell_{i,j}(\phi_{i,j}) = \ell^0_{i,j} f^{\sigma}_{i,j}(\phi_{i,j}) = \sqrt{\frac{\kappa^0}{m f_{0,interf}(\gamma_{i,j})}} f^{\sigma}_{i,j}(\phi_{i,j}) \tag{23b}$$

$$\mu_{i,j}(\phi) = \mu^0_{i,j} f^{\mu}_{i,j}(\phi) = \frac{L^0_{i,j}\kappa^0}{\sigma^0_{i,j}} f^{\mu}_{i,j}(\phi) = \frac{L^0_{i,j}}{g(\gamma_{i,j})}\sqrt{\frac{\kappa^0}{m}} f^{\mu}_{i,j}(\phi), \tag{23c}$$

where the same procedure as for the new model can be used to determine κ^0, m, $\gamma_{i,j}$ and $L^0_{i,j}$ from a set of $\sigma^0_{i,j}$ and $\mu^0_{i,j}$ and a base diffuse interface width $\ell^0_{i,j}$ for one of the boundaries. Equation (28b) shows that for this formulation the diffuse interface width also varies along the boundary with inclination. Since the inclination dependence of the grain boundary energy is introduced through the gradient term, parts with a higher energy will have a wider diffuse interface width.

B. Multiplication of whole free energy density expression with inclination dependent factor

In this alternative, inclination dependence of the grain boundary energies is introduced by multiplying the overal expression of the free energy density in the integral with

an inclination dependent factor, namely

$$F = \int_V \Bigg[A(\phi) \Bigg(m_0 f_0(\eta_1, \eta_2, \ldots, \eta_p) + \frac{\kappa_0}{2} \sum_{i=1}^{p} (\nabla \eta_i)^2 \Bigg) \Bigg] \mathrm{d}V = \int_V \Bigg[m_0 A(\phi) f_0(\eta_1, \eta_2, \ldots, \eta_p) + \frac{\kappa_0 A(\phi)}{2} \sum_{i=1}^{p} (\nabla \eta_i)^2 \Bigg] \mathrm{d}V, \tag{24}$$

with

$$A(\phi) = \frac{\sum_{i=1}^{p} \sum_{j>i}^{p} \left[f_{i,j}^{\sigma}(\phi_{i,j}) \right] \eta_i^2 \eta_j^2}{\sum_{i=1}^{p} \sum_{j>i}^{p} \eta_i^2 \eta_j^2} \tag{25}$$

The inlincation dependence of the grain boundary mobility is introduced through the kinetic coefficients $L_{i,j}$ in expression (2),

$$L_{i,j}(\phi_{i,j}) = L_{i,j}^0 f_{i,j}^{\mu}(\phi_{i,j}) \tag{26}$$

The evolution equations for the phase-field variables η_i are obtained in a fully variation way starting from Eq. (1) and using Eq. (24) for the free energy functional F, giving

$$\begin{aligned} \frac{\partial \eta_i(\mathbf{r},t)}{\partial t} = -L(\eta_1, \eta_2, \ldots, \eta_p) \Bigg[& m_0 A(\phi) \left(\eta_i^3 - \eta_i + 2\eta_i \sum_{j \neq i}^{p} \gamma_{i,j} \eta_j^2 \right) \\ & + \frac{\partial A(\phi)}{\partial \eta_i} \left(m_0 f_0(\eta_1, \ldots, \eta_p) + \frac{\kappa_0}{2} \sum_{i=1}^{p} (\nabla \eta_i)^2 \right) \\ & - \nabla \cdot \Bigg(\kappa_0 A(\phi) \nabla \eta_i \\ & + \frac{\partial A(\phi)}{\partial \nabla \eta_i} \left[m_0 f_0(\eta_1, \ldots, \eta_p) + \frac{\kappa_0}{2} \sum_{i=1}^{p} (\nabla \eta_i)^2 \right] \Bigg) \Bigg]. \end{aligned} \tag{27}$$

The parameters κ_0 and m_0 are the same for all boundaries. In the factor $A(\phi)$, the inclination dependence of the energy each type of boundary $f_{i,j}^{\sigma}(\phi_{i,j})$ is considered using the expression with the cross products of the phase-field variables. Since the inclination dependent factor is now introduced in both the gradient and the homogeneous part of the free energy density, it follows from relations (8) that the inclination dependent factor of the grain boundary energy ($f_{i,j}^{\sigma}(\phi_{i,j})$) can be introduced directly in the expression of $A(\phi)$ and the expected inclination dependence for $\sigma_{i,j}$ will be reproduced, since $\sigma_{i,j}$ is proportional to $\sqrt{\kappa_0(f_{i,j}^{\sigma}(\phi_{i,j}))m_0(f_{i,j}^{\sigma}(\phi_{i,j}))} = \sqrt{\kappa_0 m_0}(f_{i,j}^{\sigma}(\phi_{i,j}))$ (see Eq. (8a)). The inclination depence of the grain boundary mobility $f_{i,j}^{\mu}$ can be introduced directly in the kinetic coefficients $L_{i,j}$ since $\mu_{i,j}$ is proportional to $L_{i,j}$.

For this model, the following parameter relations are obtained

$$\sigma_{i,j}(\phi_{i,j}) = \sigma_{i,j}^0 f_{i,j}^{\sigma}(\phi_{i,j}) = g(\gamma_{i,j}) \sqrt{\kappa^0 m} f_{i,j}^{\sigma}(\phi_{i,j}) \tag{28a}$$

$$\ell_{i,j} = \sqrt{\frac{\kappa^0}{m f_{0,interf}(\gamma_{i,j})}} \tag{28b}$$

$$\mu_{i,j}(\phi) = \mu_{i,j}^0 f_{i,j}^{\mu}(\phi) = \frac{L_{i,j}^0 \kappa^0}{\sigma_{i,j}^0} f_{i,j}^{\mu}(\phi) = \frac{L_{i,j}^0}{g(\gamma_{i,j})} \sqrt{\frac{\kappa^0}{m}} f_{i,j}^{\mu}(\phi), \tag{28c}$$

where the same procedure as for the new model can be used to determine κ^0, m, $\gamma_{i,j}$ and $L_{i,j}^0$ from a set of $\sigma_{i,j}^0$ and $\mu_{i,j}^0$ and a minimum diffuse interface width $\ell_{i,j}$ for the grain boundary with the highest energy. Equation (28b) shows that, different from the first variant, for this formulation the diffuse interface width remains along the boundary with inclination.

advantages of this second alternatvie are therefore that the diffuse interface width remains constant along the boundary and that the inclination dependence of the model parameters follows exactely that of the grain boundary energy and mobility. The model formulation is slightly more complex.

C. Through $\gamma_{i,j}$ parameters

In this alternative, the inclination dependence of the grain boundary energies is introduced to the $\gamma_{i,j}$ coefficients only and κ and m are kept constant to certainly omit any spurious phase at grain boundaries.

The free energy functional F has the form

$$F = \int_V \Bigg[m f_0(\eta_1, \eta_2, \ldots, \eta_p) + \frac{\kappa}{2} \sum_{i=1}^{p} (\nabla \eta_i)^2 \Bigg] \mathrm{d}V, \tag{29}$$

with

$$f_0(\eta_1, \eta_2, \ldots, \eta_p) = \sum_{i=1}^{p} \left(\frac{\eta_i^4}{4} - \frac{\eta_i^2}{2} \right) + \sum_{i=1}^{p} \sum_{j>i}^{p} \gamma_{i,j}(\phi) \eta_i^2 \eta_j^2 + \frac{1}{4}. \tag{30}$$

It follows from the parameter relation xx that the inclination dependen of $\gamma_{i,j}(\phi_{i,j})$ should be such that $g(\gamma_{i,j}(\phi_{i,j}))$ follows the inclination dependence of $\sigma_{i,j}$. Hence, we take, for example,

$$g(\gamma_{i,j}) = f_{i,j}^{\sigma} = 1 + \delta_{i,j} \cos\left(n_{i,j} \left(\phi'_{i,j} - \phi_0 \right) \right) \tag{31}$$

D. Numerical simulations

iso met verschillende inclination dependence; cos 0.5 en 0 en

$$\pi/4$$

; het vierkant en zelfde orientaties; vgl met elkaar;

de vb om te tonen dat er geen spurious phases zijn

polycrystalline structure; allen zelfde energie en incl dependence (1 keer allen in zelfde rich; een kaar met gedraaid); een lage energie met inclination dependence, andere hogere energy

E. Evaluation and discussion

Comparison of the 3 alternatives.

Importance

Refer to sharp interface models.

This sample document demonstrates proper use of REVTEX 4.2 (and LATEX 2_ε) in mansucripts prepared for submission to APS journals. Further information can be found in the REVTEX 4.2 documentation included in the distribution or available at `http://journals.aps.org/revtex/`.

When commands are referred to in this example file, they are always shown with their required arguments, using normal TEX format. In this format, `#1`, `#2`, etc. stand for required author-supplied arguments to commands. For example, in `\section{#1}` the `#1` stands for the title text of the author's section heading, and in `\title{#1}` the `#1` stands for the title text of the paper.

Line breaks in section headings at all levels can be introduced using \\. A blank input line tells TEX that the paragraph has ended. Note that top-level section headings are automatically uppercased. If a specific letter or word should appear in lowercase instead, you must escape it using `\lowercase{#1}` as in the word "via" above.

F. Second-level heading: Formatting

This file may be formatted in either the `preprint` or `reprint` style. `reprint` format mimics final journal output. Either format may be used for submission purposes. `letter` sized paper should be used when submitting to APS journals.

1. Wide text (A level-3 head)

The `widetext` environment will make the text the width of the full page, as on page 11. (Note the use the `\pageref{#1}` command to refer to the page number.)

a. Note (Fourth-level head is run in) The width-changing commands only take effect in two-column formatting. There is no effect if text is in a single column.

G. Citations and References

A citation in text uses the command `\cite{#1}` or `\onlinecite{#1}` and refers to an entry in the bibliography. An entry in the bibliography is a reference to another document.

1. Citations

Because REVTEX uses the `natbib` package of Patrick Daly, the entire repertoire of commands in that package are available for your document; see the `natbib` documentation for further details. Please note that REVTEX requires version 8.31a or later of `natbib`.

a. Syntax The argument of `\cite` may be a single *key*, or may consist of a comma-separated list of keys. The citation *key* may contain letters, numbers, the dash (-) character, or the period (.) character. New with natbib 8.3 is an extension to the syntax that allows for a star (*) form and two optional arguments on the citation key itself. The syntax of the `\cite` command is thus (informally stated)

`\cite {` *key* `}`, or
`\cite {` *optarg+key* `}`, or
`\cite {` *optarg+key* `,` *optarg+key*`...}`,
where *optarg+key* signifies

key, or
`*`*key*, or
`[`*pre*`]`*key*, or
`[`*pre*`][`*post*`]`*key*, or even
`*[`*pre*`][`*post*`]`*key*.
where *pre* and *post* is whatever text you wish to place at the beginning and end, respectively, of the bibliographic reference (see Ref. [1] and the two under Ref. [2]). (Keep in mind that no automatic space or punctuation is applied.) It is highly recommended that you put the entire *pre* or *post* portion within its own set of braces, for example: `\cite { [ {`*text*`}]`*key*`}`. The extra set of braces will keep LATEX out of trouble if your *text* contains the comma (,) character.

The star (*) modifier to the *key* signifies that the reference is to be merged with the previous reference into a single bibliographic entry, a common idiom in APS and AIP articles (see below, Ref. [2]). When references are merged in this way, they are separated by a semicolon instead of the period (full stop) that would otherwise appear.

b. Eliding repeated information When a reference is merged, some of its fields may be elided: for example, when the author matches that of the previous reference, it is omitted. If both author and journal match, both are omitted. If the journal matches, but the author does not, the journal is replaced by *ibid.*, as exemplified by Ref. [2]. These rules embody common editorial practice in APS and AIP journals and will only be in effect if the

markup features of the APS and AIP BibTEX styles is employed.

c. The options of the cite command itself Please note that optional arguments to the *key* change the reference in the bibliography, not the citation in the body of the document. For the latter, use the optional arguments of the `\cite` command itself: `\cite *[`*pre-cite*`][`*post-cite*`]{`*key-list*`}`.

2. Example citations

By default, citations are numerical[3]. Author-year citations are used when the journal is RMP. To give a textual citation, use `\onlinecite{#1}`: Refs. 1 and 4. By default, the `natbib` package automatically sorts your citations into numerical order and "compresses" runs of three or more consecutive numerical citations. REVTEX provides the ability to automatically change the punctuation when switching between journal styles that provide citations in square brackets and those that use a superscript style instead. This is done through the `citeautoscript` option. For instance, the journal style `prb` automatically invokes this option because *Physical Review B* uses superscript-style citations. The effect is to move the punctuation, which normally comes after a citation in square brackets, to its proper position before the superscript. To illustrate, we cite several together [1, 2, 4–6], and once again in different order (Refs. [1, 2, 4–6]). Note that the citations were both compressed and sorted. Futhermore, running this sample file under the `prb` option will move the punctuation to the correct place.

When the `prb` class option is used, the `\cite{#1}` command displays the reference's number as a superscript rather than in square brackets. Note that the location of the `\cite{#1}` command should be adjusted for the reference style: the superscript references in `prb` style must appear after punctuation; otherwise the reference must appear before any punctuation. This sample was written for the regular (non-`prb`) citation style. The command `\onlinecite{#1}` in the `prb` style also displays the reference on the baseline.

3. References

A reference in the bibliography is specified by a `\bibitem{#1}` command with the same argument as the `\cite{#1}` command. `\bibitem{#1}` commands may be crafted by hand or, preferably, generated by BibTEX. REVTEX 4.2 includes BibTEX style files `apsrev4-2.bst`, `apsrmp4-2.bst` appropriate for *Physical Review* and *Reviews of Modern Physics*, respectively.

4. Example references

This sample file employs the `\bibliography` command, which formats the `output.bbl` file and specifies which bibliographic databases are to be used by BibTEX (one of these should be by arXiv convention `output.bib`). Running BibTEX (via `bibtex output`) after the first pass of LATEX produces the file `output.bbl` which contains the automatically formatted `\bibitem` commands (including extra markup information via `\bibinfo` and `\bibfield` commands). If not using BibTEX, you will have to create the `thebibiliography` environment and its `\bibitem` commands by hand.

Numerous examples of the use of the APS bibliographic entry types appear in the bibliography of this sample document. You can refer to the `output.bib` file, and compare its information to the formatted bibliography itself.

H. Footnotes

Footnotes, produced using the `\footnote{#1}` command, usually integrated into the bibliography alongside the other entries. Numerical citation styles do this[7]; author-year citation styles place the footnote at the bottom of the text column. Note: due to the method used to place footnotes in the bibliography, *you must re-run BibTEX every time you change any of your document's footnotes.*

V. MATH AND EQUATIONS

Inline math may be typeset using the `$` delimiters. Bold math symbols may be achieved using the `bm` package and the `\bm{#1}` command it supplies. For instance, a bold α can be typeset as `$\bm{\alpha}$` giving $\boldsymbol{\alpha}$. Fraktur and Blackboard (or open face or double struck) characters should be typeset using the `\mathfrak{#1}` and `\mathbb{#1}` commands respectively. Both are supplied by the `amssymb` package. For example, `$\mathbb{R}$` gives $\mathbb{R}$ and `$\mathfrak{G}$` gives $\mathfrak{G}$

In LATEX there are many different ways to display equations, and a few preferred ways are noted below. Displayed math will center by default. Use the class option `fleqn` to flush equations left.

Below we have numbered single-line equations; this is the most common type of equation in *Physical Review*:

$$\chi_+(p) \lesssim [2|\mathbf{p}|(|\mathbf{p}|+p_z)]^{-1/2} \begin{pmatrix} |\mathbf{p}|+p_z \\ px+ip_y \end{pmatrix}, \quad (32)$$

$$\left\{ \mathbb{1}234567890abc123\alpha\beta\gamma\delta1234556\alpha\beta \frac{1\sum_b^a}{A^2} \right\}. \quad (33)$$

Note the open one in Eq. (33).

Not all numbered equations will fit within a narrow column this way. The equation number will move down

automatically if it cannot fit on the same line with a one-line equation:

$$\left\{ab12345678abc123456abcdef\alpha\beta\gamma\delta1234556\alpha\beta\frac{1\sum_b^a}{A^2}\right\}. \tag{34}$$

When the `\label{#1}` command is used [cf. input for Eq. (33)], the equation can be referred to in text without knowing the equation number that TEX will assign to it. Just use `\ref{#1}`, where `#1` is the same name that used in the `\label{#1}` command.

Unnumbered single-line equations can be typeset using the `\[`, `\]` format:

$$g^+g^+ \to g^+g^+g^+g^+\dots\ ,\quad q^+q^+ \to q^+g^+g^+\dots\ .$$

A. Multiline equations

Multiline equations are obtained by using the `eqnarray` environment. Use the `\nonumber` command at the end of each line to avoid assigning a number:

$$\begin{aligned}\mathcal{M} =& ig_Z^2(4E_1E_2)^{1/2}(l_i^2)^{-1}\delta_{\sigma_1,-\sigma_2}(g^e_{\sigma_2})^2\chi_{-\sigma_2}(p_2)\\ &\times[\epsilon_j l_i\epsilon_i]_{\sigma_1}\chi_{\sigma_1}(p_1),\end{aligned} \tag{35}$$

$$\begin{aligned}\sum|M_g^{\rm viol}|^2 =& g_S^{2n-4}(Q^2)\ N^{n-2}(N^2-1)\\ &\times\left(\sum_{i<j}\right)\sum_{\rm perm}\frac{1}{S_{12}}\frac{1}{S_{12}}\sum_\tau c_\tau^f\ .\end{aligned} \tag{36}$$

Note: Do not use `\label{#1}` on a line of a multiline equation if `\nonumber` is also used on that line. Incorrect cross-referencing will result. Notice the use `\text{#1}` for using a Roman font within a math environment.

To set a multiline equation without *any* equation numbers, use the `\begin{eqnarray*}`, `\end{eqnarray*}` format:

$$\begin{aligned}\sum|M_g^{\rm viol}|^2 =& g_S^{2n-4}(Q^2)\ N^{n-2}(N^2-1)\\ &\times\left(\sum_{i<j}\right)\left(\sum_{\rm perm}\frac{1}{S_{12}S_{23}S_{n1}}\right)\frac{1}{S_{12}}\ .\end{aligned}$$

To obtain numbers not normally produced by the automatic numbering, use the `\tag{#1}` command, where `#1` is the desired equation number. For example, to get an equation number of (2.6′),

$$g^+g^+ \to g^+g^+g^+g^+\dots\ ,\quad q^+q^+ \to q^+g^+g^+\dots\ . \tag{2.6′}$$

a. A few notes on `tags` `\tag{#1}` requires the `amsmath` package. Place the `\tag{#1}` command before the `\label{#1}`, if any. The numbering produced by `\tag{#1}` *does not affect* the automatic numbering in REVTEX; therefore, the number must be known ahead of time, and it must be manually adjusted if other equations are added. `\tag{#1}` works with both single-line and multiline equations. `\tag{#1}` should only be used in exceptional cases—do not use it to number many equations in your paper. Please note that this feature of the `amsmath` package is *not* compatible with the `hyperref` (6.77u) package.

Enclosing display math within `\begin{subequations}` and `\end{subequations}` will produce a set of equations that are labeled with letters, as shown in Eqs. (37b) and (37a) below. You may include any number of single-line and multiline equations, although it is probably not a good idea to follow one display math directly after another.

$$\begin{aligned}\mathcal{M} =& ig_Z^2(4E_1E_2)^{1/2}(l_i^2)^{-1}(g^e_{\sigma_2})^2\chi_{-\sigma_2}(p_2)\\ &\times[\epsilon_i]_{\sigma_1}\chi_{\sigma_1}(p_1).\end{aligned} \tag{37a}$$

$$\left\{abc123456abcdef\alpha\beta\gamma\delta1234556\alpha\beta\frac{1\sum_b^a}{A^2}\right\}, \tag{37b}$$

Giving a `\label{#1}` command directly after the `\begin{subequations}`, allows you to reference all the equations in the `subequations` environment. For example, the equations in the preceding subequations environment were Eqs. (37).

1. Wide equations

The equation that follows is set in a wide format, i.e., it spans the full page. The wide format is reserved for long equations that cannot easily be set in a single column:

$$\mathcal{R}^{(\rm d)} = g^e_{\sigma_2}\left(\frac{[\Gamma^Z(3,21)]_{\sigma_1}}{Q_{12}^2-M_W^2}+\frac{[\Gamma^Z(13,2)]_{\sigma_1}}{Q_{13}^2-M_W^2}\right)+x_WQ_e\left(\frac{[\Gamma^\gamma(3,21)]_{\sigma_1}}{Q_{12}^2-M_W^2}+\frac{[\Gamma^\gamma(13,2)]_{\sigma_1}}{Q_{13}^2-M_W^2}\right)\ . \tag{38}$$

This is typed to show how the output appears in wide format. (Incidentally, since there is no blank line between the `equation` environment above and the start of this paragraph, this paragraph is not indented.)

VI. CROSS-REFERENCING

REVTEX will automatically number such things as sections, footnotes, equations, figure captions, and table captions. In order to reference them in text, use the `\label{#1}` and `\ref{#1}` commands. To reference a particular page, use the `\pageref{#1}` command.

The `\label{#1}` should appear within the section heading, within the footnote text, within the equation, or within the table or figure caption. The `\ref{#1}` command is used in text at the point where the reference is to be displayed. Some examples: Section I on page 1, Table IV, and Fig. 4.

VII. FLOATS: FIGURES, TABLES, VIDEOS, ETC.

Figures and tables are usually allowed to "float", which means that their placement is determined by LaTeX, while the document is being typeset.

Use the `figure` environment for a figure, the `table` environment for a table. In each case, use the `\caption` command within to give the text of the figure or table caption along with the `\label` command to provide a key for referring to this figure or table. The typical content of a figure is an image of some kind; that of a table is an alignment.

Insert an image using either the `graphics` or `graphix` packages, which define the `\includegraphics{#1}` command. (The two packages differ in respect of the optional arguments used to specify the orientation, scaling, and translation of the image.) To create an alignment, use the `tabular` environment.

The best place to locate the `figure` or `table` environment is immediately following its first reference in text; this sample document illustrates this practice for Fig. 4, which shows a figure that is small enough to fit in a single column.

In exceptional cases, you will need to move the float earlier in the document, as was done with Table V:

TABLE IV. A table that fits into a single column of a two-column layout. Note that REVTEX 4 adjusts the intercolumn spacing so that the table fills the entire width of the column. Table captions are numbered automatically. This table illustrates left-, center-, decimal- and right-aligned columns, along with the use of the `ruledtabular` environment which sets the Scotch (double) rules above and below the alignment, per APS style.

Left[a]	Centered[b]	Decimal	Right
1	2	3.001	4
10	20	30	40
100	200	300.0	400

[a] Note a.
[b] Note b.

LaTeX's float placement algorithms need to know about a full-page-width float earlier.

Fig. 5 has content that is too wide for a single column, so the `figure*` environment has been used.

The content of a table is typically a `tabular` environment, giving rows of type in aligned columns. Column entries separated by `&`'s, and each row ends with \\. The required argument for the `tabular` environment specifies how data are aligned in the columns. For instance, entries may be centered, left-justified, right-justified, aligned on a decimal point. Extra column-spacing may be be specified as well, although REVTEX 4 sets this spacing so that the columns fill the width of the table. Horizontal rules are typeset using the `\hline` command. The doubled (or Scotch) rules that appear at the top and bottom of a table can be achieved enclosing the `tabular` environment within a `ruledtabular` environment. Rows whose columns span multiple columns can be typeset using the `\multicolumn{#1}{#2}{#3}` command (for example, see the first row of Table V).

Tables IV, V, VI, and VII show various effects. A table that fits in a single column employs the `table` environment. Table V is a wide table, set with the `table*` environment. Long tables may need to break across pages. The most straightforward way to accomplish this is to specify the `[H]` float placement on the `table` or `table*` environment. However, the LaTeX 2_ε package `longtable` allows headers and footers to be specified for each page of the table. A simple example of the use of `longtable` can be found in the file `summary.tex` that is included with the REVTEX 4 distribution.

There are two methods for setting footnotes within a table (these footnotes will be displayed directly below the table rather than at the bottom of the page or in the bibliography). The easiest and preferred method is just to use the `\footnote{#1}` command. This will automatically enumerate the footnotes with lowercase roman letters. However, it is sometimes necessary to have multiple entries in the table share the same footnote. In this case, there is no choice but to manually create the footnotes using `\footnotemark[#1]` and `\footnotetext[#1]{#2}`. `#1` is a numeric value. Each time the same value for `#1` is used, the same mark is produced in the table. The `\footnotetext[#1]{#2}` commands are placed after the

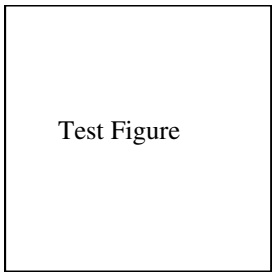

FIG. 4. A figure caption. The figure captions are automatically numbered.

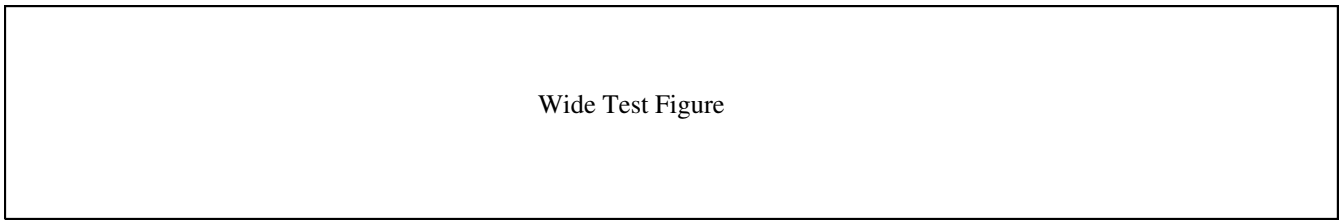

FIG. 5. Use the figure* environment to get a wide figure that spans the page in `twocolumn` formatting.

TABLE V. This is a wide table that spans the full page width in a two-column layout. It is formatted using the `table*` environment. It also demonstates the use of `\multicolumn` in rows with entries that span more than one column.

	D^1_{4h}		D^5_{4h}	
Ion	1st alternative	2nd alternative	lst alternative	2nd alternative
K	$(2e)+(2f)$	$(4i)$	$(2c)+(2d)$	$(4f)$
Mn	$(2g)$[a]	$(a)+(b)+(c)+(d)$	$(4e)$	$(2a)+(2b)$
Cl	$(a)+(b)+(c)+(d)$	$(2g)$[a]	$(4e)$[a]	
He	$(8r)$[a]	$(4j)$[a]	$(4g)$[a]	
Ag		$(4k)$[a]		$(4h)$[a]

[a] The z parameter of these positions is $z \sim \frac{1}{4}$.

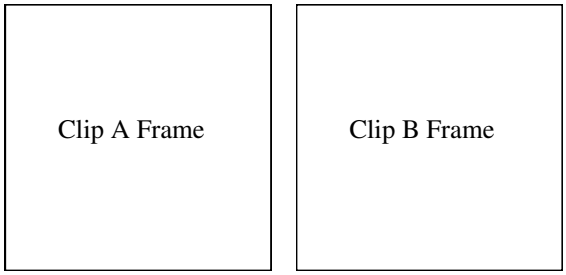

Video 1. Students explain their initial idea about Newton's third law to a teaching assistant. Clip (a): same force. Clip (b): move backwards.

`tabular` environment. Examine the LaTeX source and output for Tables IV and VII for examples.

Video 1 illustrates several features new with REVTeX4.2, starting with the `video` environment, which is in the same category with `figure` and `table`. The `\setfloatlink` command causes the title of the video to be a hyperlink to the indicated URL; it may be used with any environment that takes the `\caption` command. The `\href` command has the same significance as it does in the context of the `hyperref` package: the second argument is a piece of text to be typeset in your document; the first is its hyperlink, a URL.

Physical Review style requires that the initial citation of figures or tables be in numerical order in text, so don't cite Fig. 5 until Fig. 4 has been cited.

TABLE VI. Numbers in columns Three–Five are aligned with the "d" column specifier (requires the `dcolumn` package). Non-numeric entries (those entries without a ".") in a "d" column are aligned on the decimal point. Use the "D" specifier for more complex layouts.

One	Two	Three	Four	Five
one	two	three	four	five
He	2	2.77234	45672.	0.69
C[a]	C[b]	12537.64	37.66345	86.37

[a] Some tables require footnotes.
[b] Some tables need more than one footnote.

TABLE VII. A table with numerous columns that still fits into a single column. Here, several entries share the same footnote. Inspect the LaTeX input for this table to see exactly how it is done.

	r_c (Å)	r_0 (Å)	κr_0		r_c (Å)	r_0 (Å)	κr_0
Cu	0.800	14.10	2.550	Sn[a]	0.680	1.870	3.700
Ag	0.990	15.90	2.710	Pb[b]	0.450	1.930	3.760
Au	1.150	15.90	2.710	Ca[c]	0.750	2.170	3.560
Mg	0.490	17.60	3.200	Sr[d]	0.900	2.370	3.720
Zn	0.300	15.20	2.970	Li[b]	0.380	1.730	2.830
Cd	0.530	17.10	3.160	Na[e]	0.760	2.110	3.120
Hg	0.550	17.80	3.220	K[e]	1.120	2.620	3.480
Al	0.230	15.80	3.240	Rb[c]	1.330	2.800	3.590
Ga	0.310	16.70	3.330	Cs[d]	1.420	3.030	3.740
In	0.460	18.40	3.500	Ba[e]	0.960	2.460	3.780
Tl	0.480	18.90	3.550				

[a] Here's the first, from Ref. 2.
[b] Here's the second.
[c] Here's the third.
[d] Here's the fourth.
[e] And etc.

ACKNOWLEDGMENTS

We wish to acknowledge the support of the author community in using REVTEX, offering suggestions and encouragement, testing new versions, ...

Appendix A: Appendixes

To start the appendixes, use the `\appendix` command. This signals that all following section commands refer to appendixes instead of regular sections. Therefore, the `\appendix` command should be used only once—to setup the section commands to act as appendixes. Thereafter normal section commands are used. The heading for a section can be left empty. For example,

```
\appendix
\section{}
```

will produce an appendix heading that says "APPENDIX A" and

```
\appendix
\section{Background}
```

will produce an appendix heading that says "APPENDIX A: BACKGROUND" (note that the colon is set automatically).

If there is only one appendix, then the letter "A" should not appear. This is suppressed by using the star version of the appendix command (`\appendix*` in the place of `\appendix`).

Appendix B: A little more on appendixes

Observe that this appendix was started by using

```
\section{A little more on appendixes}
```

Note the equation number in an appendix:

$$E = mc^2. \tag{B1}$$

1. A subsection in an appendix

You can use a subsection or subsubsection in an appendix. Note the numbering: we are now in Appendix B 1.

Note the equation numbers in this appendix, produced with the subequations environment:

$$E = mc, \tag{B2a}$$
$$E = mc^2, \tag{B2b}$$
$$E \gtrsim mc^3. \tag{B2c}$$

They turn out to be Eqs. (B2a), (B2b), and (B2c).

[1] E. Witten, (2001), hep-th/0106109, and references therein

[2] See the explanation of time travel in R. P. Feynman, Phys. Rev. **94**, 262 (1954); The classical relativistic treatment of A. Einstein, Yu. Podolsky, and N. Rosen (EPR), *ibid.* **47**, 777 (1935) is a relative classic

[3] E. Beutler, in *Williams Hematology*, Vol. 2, edited by E. Beutler, M. A. Lichtman, B. W. Coller, and T. S. Kipps (McGraw-Hill, New York, 1994) Chap. 7, pp. 654–662, 5th ed.

[4] N. D. Birell and P. C. W. Davies, *Quantum Fields in Curved Space* (Cambridge University Press, 1982).

[5] J. G. P. Berman and J. F. M. Izrailev, Stability of nonlinear modes, Physica D **88**, 445 (1983).

[6] E. B. Davies and L. Parns, Trapped modes in acoustic waveguides, Q. J. Mech. Appl. Math. **51**, 477 (1988).

[7] Automatically placing footnotes into the bibliography requires using BibTeX to compile the bibliography.

[8] E. Beutler, in *Williams Hematology*, Vol. 2, edited by E. Beutler, M. A. Lichtman, B. W. Coller, and T. S. Kipps (McGraw-Hill, New York, 1994) 5th ed., Chap. 7, pp. 654–662.

[9] D. E. Knuth, in *Fundamental Algorithms*, The Art of Computer Programming, Vol. 1 (Addison-Wesley, Reading, Massachusetts, 1973) Section 1.2, pp. 10–119, 2nd ed., a full INBOOK entry.

[10] J. S. Smith and G. W. Johnson, Philos. Trans. R. Soc. London, Ser. B **777**, 1395 (2005).

[11] W. J. Smith, T. J. Johnson, and B. G. Miller, Surface chemistry and preferential crystal orientation on a silicon surface (2010), J. Appl. Phys. (unpublished).

[12] V. K. Smith, K. Johnson, and M. O. Klein, Surface chemistry and preferential crystal orientation on a silicon surface (2010), J. Appl. Phys. (submitted).

[13] U. Ünderwood, N. Ñet, and P. P̄ot, Lower bounds for wishful research results (1988), talk at Fanstord University (A full UNPUBLISHED entry).

[14] M. P. Johnson, K. L. Miller, and K. Smith, personal communication (2007).

[15] J. Smith, ed., *AIP Conf. Proc.*, Vol. 841 (2007).

[16] W. V. Oz and M. Yannakakis, eds., *Proc. Fifteenth Annual*, All ACM Conferences No. 17, ACM (Academic Press, Boston, 1983) a full PROCEEDINGS entry.

[17] Y. Burstyn, Proceedings of the 5th International Molecular Beam Epitaxy Conference, Santa Fe, NM (2004), (unpublished).

[18] B. Quinn, ed., *Proceedings of the 2003 Particle Accelerator Conference, Portland, OR, 12-16 May 2005* (Wiley, New York, 2001) albeit the conference was held in 2005, it was the 2003 conference, and the proceedings were published in 2001; go figure.

[19] A. G. Agarwal, Proceedings of the Fifth Low Temperature Conference, Madison, WI, 1999, Semiconductors **66**, 1238 (2001).

[20] R. Smith, Hummingbirds are our friends, J. Appl. Phys. (these proceedings) (2001), abstract No. DA-01.

[21] J. Smith, Proc. SPIE **124**, 367 (2007), required title is missing.

[22] T. Térrific, *An $O(n \log n / \log \log n)$ Sorting Algorithm*, Wishful Research Result 7 (Fanstord University, Computer Science Department, Fanstord, California, 1988) a full TECHREPORT entry.

[23] J. Nelson, TWI Report 666/1999 (Jan. 1999) required institution missing.

[24] W. K. Fields, ECE Report No. AL944 (2005) required institution missing.

[25] Y. M. Zalkins, e-print arXiv:cond-mat/040426 (2008).

[26] J. Nelson, U.S. Patent No. 5,693,000 (12 Dec. 2005).

[27] J. K. Nelson, M.S. thesis, New York University (1999).

[28] É. Masterly, *Mastering Thesis Writing*, Master's project, Stanford University, English Department (1988), a full MASTERSTHESIS entry.

[29] S. M. Smith, Ph.D. thesis, Massachusetts Institute of Technology (2003).

[30] S. R. Kawa and S.-J. Lin, J. Geophys. Res. **108**, 4201 (2003), DOI:10.1029/2002JD002268.

[31] F. P. Phony-Baloney, *Fighting Fire with Fire: Festooning French Phrases*, PhD dissertation, Fanstord University, Department of French (1988), a full PHDTHESIS entry.

[32] D. E. Knuth, *Seminumerical Algorithms*, 2nd ed., The Art of Computer Programming, Vol. 2 (Addison-Wesley, Reading, Massachusetts, 1981) a full BOOK entry.

[33] J. C. Knvth, The programming of computer art, Vernier Art Center, Stanford, California (1988), a full BOOKLET entry.

[34] R. Ballagh and C. Savage, Bose-einstein condensation: from atomic physics to quantum fluids, proceedings of the 13th physics summer school (World Scientific, Singapore, 2000) cond-mat/0008070.

[35] R. Ballagh and C. Savage, Bose-einstein condensation: from atomic physics to quantum fluids, in *Proceedings of the 13th Physics Summer School*, edited by C. Savage and M. Das (World Scientific, Singapore, 2000) cond-mat/0008070.

[36] W. Opechowski and R. Guccione, Introduction to the theory of normal metals, in *Magnetism*, Vol. IIa, edited by G. T. Rado and H. Suhl (Academic Press, New York, 1965) p. 105.

[37] W. Opechowski and R. Guccione, Introduction to the theory of normal metals, in *Magnetism*, Vol. IIa, edited by G. T. Rado and H. Suhl (Academic Press, New York, 1965) p. 105.

[38] W. Opechowski and R. Guccione, Introduction to the theory of normal metals, in *Magnetism*, Vol. IIa, edited by G. T. Rado and H. Suhl (Academic Press, New York, 1965) p. 105.

[39] J. M. Smith, Molecular dynamics (Academic, New York, 1980).

[40] V. E. Zakharov and A. B. Shabat, Exact theory of two-dimensional self-focusing and one-dimensional self-modulation of waves in nonlinear media, Zh. Eksp. Teor. Fiz. **61**, 118 (1971), [Sov. Phys. JETP **34**, 62 (1972)].

[41] J. M. Smith, in *Molecular Dynamics*, edited by C. Brown (Academic, New York, 1980).

[42] D. D. Lincoll, Semigroups of recurrences, in *High Speed Computer and Algorithm Organization*, Fast Computers No. 23, edited by D. J. Lipcoll, D. H. Lawrie, and A. H. Sameh (Academic Press, New York, 1977) 3rd ed., Part 3, pp. 179–183, a full INCOLLECTION entry.

[43] A. V. Oaho, J. D. Ullman, and M. Yannakakis, On notions of information transfer in VLSI circuits, in *Proc. Fifteenth Annual ACM*, Boston, 1982, All ACM Conferences No. 17, edited by W. V. Oz and M. Yannakakis, ACM (Academic Press, New York, 1983) pp. 133–139, a full INPROCEDINGS entry.

[44] L. Manmaker, *The Definitive Computer Manual*, Chips-R-Us, Silicon Valley, silver ed. (1986), a full MANUAL entry.